Available online at www.sciencedirect.com

ScienceDirect

Proceedings of the Combustion Institute 36 (2017) 3587–3596

Proceedings of the Combustion Institute

www.elsevier.com/locate/proci

Ignition of a lean PRF/air mixture under RCCI/SCCI conditions: Chemical aspects

Minh Bau Luong [a], Gwang Hyeon Yu [a], Suk Ho Chung [b], Chun Sang Yoo [a,c,*]

[a] *Department of Mechanical Engineering, Ulsan National Institute of Science and Technology, Ulsan 689–798, Republic of Korea*

[b] *Clean Combustion Research Center, King Abdullah University of Science and Technology, Thuwal, Saudi Arabia*

[c] *School of Mechanical and Nuclear Engineering, Ulsan National Institute of Science and Technology, Ulsan 689–798, Republic of Korea*

Received 4 December 2015; accepted 10 June 2016
Available online 6 October 2016

Abstract

Chemical aspects of the ignition of a primary reference fuel (PRF)/air mixture under reactivity controlled compression ignition (RCCI) and stratified charge compression ignition (SCCI) conditions are investigated by analyzing two-dimensional direct numerical simulation (DNS) data with chemical explosive mode (CEM) analysis. CEMA is adopted to provide fundamental insights into the ignition process by identifying controlling species and elementary reactions at different locations and times. It is found that at the first ignition delay, low-temperature chemistry (LTC) represented by the isomerization of alkylperoxy radical, chain branching reactions of keto-hydroperoxide, and H-atom abstraction of *n*-heptane is predominant for both RCCI and SCCI combustion. In addition, explosion index and participation index analyses together with conditional means on temperature verify that low-temperature heat release (LTHR) from local mixtures with relatively-high *n*-heptane concentration occurs more intensively in RCCI combustion than in SCCI combustion, which ultimately advances the overall RCCI combustion and distributes its heat release rate over time. It is also found that at the onset of the main combustion, high-temperature heat release (HTHR) occurs primarily in thin deflagrations where temperature, CO, and OH are found to be the most important species for the combustion. The conversion reaction of CO to CO_2 and hydrogen chemistry are identified as important reactions for HTHR. The overall RCCI/SCCI combustion can be understood by mapping the variation of 2-D RCCI/SCCI combustion in temperature space onto the temporal evolution of 0-D ignition.

* Corresponding author at: Department of Mechanical Engineering, Ulsan National Institute of Science and Technology, Ulsan 44919, Republic of Korea. Fax: +82 522172409.

E-mail addresses: csyoo@unist.ac.kr, withspring@gmail.com (C.S. Yoo).

http://dx.doi.org/10.1016/j.proci.2016.06.076

Keywords: Chemical explosive mode analysis (CEMA); Direct numerical simulation (DNS); Reactivity controlled compression ignition (RCCI); Stratified charge compression ignition (SCCI); Primary reference fuel (PRF)

1. Introduction

Homogeneous-charge compression ignition (HCCI) engines have been developed because they can provide high thermal efficiency and ultra-low emissions compared to the conventional IC engines. However, the development of prototype HCCI engine has been prohibited by its narrow operating range and difficulties in combustion-phasing control. To overcome these problems, some variants of HCCI engines including reactivity controlled compression ignition (RCCI) and stratified charge compression ignition (SCCI) have been proposed thus far. To introduce in-cylinder fuel stratification, dual-fuel RCCI combustion uses in-cylinder blend of two fuels with different ignition characteristics: low reactivity fuel (e.g., *iso*-octane) supplied through port-fuel injection (PFI) and directly-injected high reactivity fuel (e.g., *n*-heptane). However, SCCI combustion uses only a single fuel with the same two-stage injection strategy. With optimized blending of two fuels rather than a single fuel, RCCI combustion can provide better combustion-phasing control with lower pressure-rise rate (PRR) [1,2].

There have been numerous experimental and computational studies of HCCI-type engines, which primarily focus on the bulk engine characteristics such as emissions and operating performances [1–10]. However, only a few studies on the chemical combustion process of RCCI/SCCI combustion have been performed [3,9,11–15]. For instance, Kokjohn et al. [3] numerically investigated the combustion characteristics of E85-diesel RCCI combustion and found that formaldehyde (CH_2O) and hydroxyl (OH) radicals are the key species for the first- and second-stage ignitions, respectively, and the less reactive fuel was consumed nearly simultaneously with formaldehyde.

From the spectroscopic and chemical-kinetic analysis of HCCI combustion, Hwang et al. [12] identified that significant amount of low-temperature heat release (LTHR) of PRF80/air mixtures occurs in the range of 760 to 880 K with significant formaldehyde production, resulting in rapid temperature rise during the intermediate-temperature heat release (ITHR) and thereby advancing the main combustion. Westbrook [11] pointed out that the overall HCCI combustion can be advanced by adopting variations in engine parameters such as pressure, temperature, and equivalence ratio which enable in-cylinder fuel/air mixtures to reach the H_2O_2 decomposition temperature at earlier time.

Recently, Vuilleumier et al. [15] found from an experimental and modeling study that the addition of highly reactive *n*-heptane content induces the increase of ITHR, eventually triggering high-temperature heat release (HTHR) with a significant formaldehyde accumulation. In addition, they identified the dominant reaction pathways: H-atom abstraction from *n*-heptane by OH and the addition of heptyl radicals to O_2. These previous studies, however, were either RANS and low-dimensional analyses or optical measurement with high uncertainty to discern individual fuel species such that further understanding of the chemical aspects of RCCI/SCCI combustion is still needed.

More recently, Luong et al. [9] investigated the ignition characteristics of *n*-heptane/air mixture under HCCI/SCCI conditions by performing 2-D direct numerical simulations (DNSs). They identified important species and reactions for HCC/SCCI combustion by using chemical explosive mode analysis (CEMA). However, CEMA has not been applied to RCCI combustion. Therefore, the objective of the present study is to provide insights into the chemical ignition process of PRF/air mixture under RCCI/SCCI conditions by analyzing 2-D DNS data with CEMA.

For this purpose, we use the data set generated from 2-D DNSs of the ignition of a lean PRF/air mixture under RCCI/SCCI conditions by Luong et al. [16]. From this study, it is found that the overall combustion of RCCI is more advanced and more distributed in time than that of SCCI due to the dominant role of reactivity stratification in inducing more deflagration mode of combustion in the low-to-intermediate temperature regime. However, both RCCI and SCCI have similar overall combustion characteristics in the high-temperature regime because the ignition of the PRF/air mixture becomes less sensitive to reactivity stratification and/or equivalence ratio.

2. Methodology

To investigate the chemical aspects of RCCI and SCCI combustion, we analyze 2-D DNS data set in [16] using CEMA. The 2-D DNSs of the ignition of the PRF/air mixture under RCCI and SCCI conditions were simulated using the Sandia compressible DNS code [17], S3D, with a

116-species reduced chemistry of PRF oxidation [7]. Note that recent theoretical and experimental findings on hydroperoxyalkyl (QOOH) chemistry [18–21] have not been updated in the present PRF reduced mechanism. However, it still shows good agreement with experimental results in terms of ignition delays, flame propagation speeds, and extinction residence times [7].

The initial conditions for DNSs are specified as follows. The initial pressure, p_0, mean equivalence ratio, ϕ_0, are 40 atm and 0.45, respectively. PRF50 (i.e., a 50% *iso*-octane and 50% *n*-heptane blend by volume) was adopted as the mean fuel for RCCI combustion and the single fuel for SCCI combustion. For RCCI cases, *n*-heptane field is initialized by $m = \overline{m} + m'$, superimposed on a uniform *iso*-octane/air mixture, where m is the mass of *n*-heptane, and the 'overbar' and $'$ represent the mean and fluctuation, respectively. For SCCI cases, PRF50 is supplied through two-stage injection and hence, m represents the mass of PRF50. The local variations in PRF number, equivalence ratio, and temperature can be achieved for RCCI combustion, while only variations in equivalence ratio and temperature are obtained for SCCI combustion. The initial turbulent flow field is generated using an isotropic kinetic energy spectrum function by Passot-Pouquet [22]. Concentration and temperature fields are also generated from the same energy spectrum as turbulence with different random number and then are superimposed on top of the turbulence field. The periodic boundary conditions are imposed in all directions, and as such, RCCI/SCCI combustion occurs in constant volume. For more details of the numerical setup, readers are referred to [16].

Two representative RCCI/SCCI cases (i.e., Case 6 for RCCI and Case 8 for SCCI in [16]) with the degree of fuel stratification, $r = m'/\overline{m} = 0.44$, temperature fluctuation, $T' = 30$ K, at the initial mean temperature, $T_0 = 900$ K, are chosen for the present CEMA such that both cases are initially involved in the low- and intermediate-temperature chemistries. The 0-D homogeneous ignition delay, τ_{ig}^0, of PRF50 is 2.2 ms. For both cases, negatively-correlated T–r field is assumed to consider the evaporative cooling effect of directly-injected fuel.

Note that CEMA has been applied to various DNS studies [23–26] to elucidate the chemical aspects of turbulent combustion and is now believed as one of the useful computational flame diagnostics tools for the systematic detection of important species and reactions in premixed flames and flame ignition/extinction. Also note that the characteristics of two-stage ignition of large hydrocarbon fuel/air mixtures have been numerically investigated by adopting the computational singular perturbation method [27] and CEMA [6–9,28–30].

CEMA is briefly explained here. For more details of CEMA, readers are referred to [23,25,29]. For a chemically-reacting system, the discretized conservation equations can be expressed as:

$$\frac{D\mathbf{y}}{Dt} = \mathbf{g}(\mathbf{y}) = \boldsymbol{\omega}(\mathbf{y}) + \mathbf{s}(\mathbf{y}), \tag{1}$$

where D/Dt is the material derivative, which can be replaced by d/dt in the Lagrangian coordinate. $\mathbf{y}$ denotes the solution variables including species concentrations and temperature. $\boldsymbol{\omega}$ and $\mathbf{s}$ represent respectively the chemical source term and all the other non-chemical source terms such as diffusion in flames and homogeneous mixing term in stirred reactors.

Since the Jacobian of the chemical source term, $\mathbf{J}_{\boldsymbol{\omega}}$ ($\equiv \partial\boldsymbol{\omega}/\partial\mathbf{y}$), retains the chemical information of local mixture, the chemical feature of the mixture can be determined based on the Jacobian. To capture the chemical feature in CEMA, a chemical mode is defined as an eigenmode of $\mathbf{J}_{\boldsymbol{\omega}}$, which is associated with an eigenvalue, λ_e, and a corresponding pair of the left and right eigenvectors, $\mathbf{a}_e$ and $\mathbf{b}_e$. Chemical explosive mode (CEM) is a chemical mode of which real part of eigenvalue is positive, $\mathrm{Re}(\lambda_e) > 0$.

In general, a local mixture with a CEM is destined to auto-ignite if there are no thermal and radical losses. Therefore, CEM indicates an intrinsic chemical feature of ignitable mixture: i.e., a mixture with $\mathrm{Re}(\lambda_e) > 0$ is more apt to ignite while a mixture with $\mathrm{Re}(\lambda_e) < 0$ is already burnt or fails to ignite.

The critical chemical kinetic processes in RCCI and SCCI combustion can further be identified by evaluating explosive index (EI) and participation index (PI) of local mixture. **EI** and **PI** are defined as [25,29]:

$$\mathbf{EI} = \frac{|\mathbf{a}_e \otimes \mathbf{b}_e^T|}{sum(|\mathbf{b}_e \otimes \mathbf{b}_e^T|)}, \tag{2}$$

$$\mathbf{PI} = \frac{|\mathbf{b}_e \cdot \mathbf{S} \otimes \mathbf{R}|}{sum(|(\mathbf{b}_e \cdot \mathbf{S}) \otimes \mathbf{R}|)}, \tag{3}$$

where $\mathbf{S}$ and $\mathbf{R}$ represent the stoichiometric coefficient matrix and the vector of the net rates for reactions, respectively. The symbol $\otimes$ represents the element-wise multiplication of two vectors. Since **EI** and **PI** indicate the normalized contribution of each variable and reaction to the CEM, respectively, and as such, controlling species and reactions for RCCI/SCCI combustion can be elucidated by evaluating **EI** and **PI** values. Since the mass fractions of quasi-steady state species in the reduced chemistry are functions of the other species, the 171-species skeletal mechanism for PRF oxidation [7] is used to analytically evaluate $\mathbf{J}_{\boldsymbol{\omega}}$, $\mathbf{a}_e$, and $\mathbf{b}_e$.

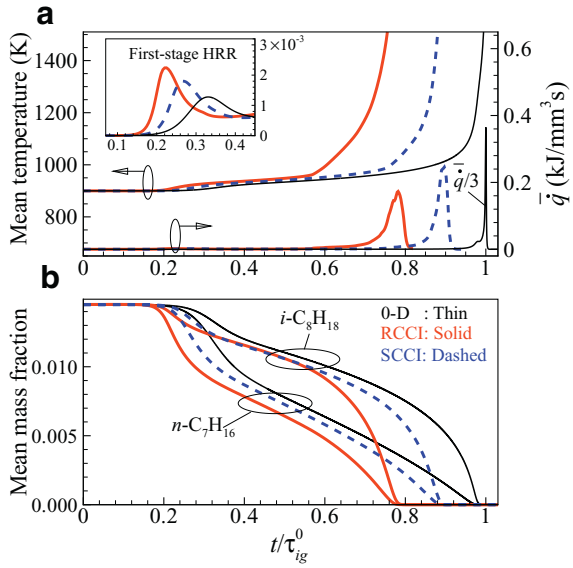

Fig. 1. Temporal evolution of (a) the mean HRR and temperature and (b) the mean mass fraction of *n*-heptane and *iso*-octane for RCCI, SCCI, and 0-D ignition.

3. Results and discussion

3.1. Overall RCCI/SCCI combustion

The characteristics of RCCI/SSCI combustion are first elucidated by examining the temporal evolution of the mean heat release rate (HRR) and temperature together with two main fuel mass fractions as shown in Fig. 1. Several points are to be noted from the figures. First, the overall RCCI combustion occurs earlier and its mean HRR is more distributed over time than the SCCI combustion. This is because local mixtures with small PRF number or relatively-high *n*-heptane concentration in RCCI case auto-ignite rapidly, which enhances deflagration mode of combustion and smoothes out the mean HRR as explained in [16].

The difference between RCCI and SCCI combustion can be explained by the consumption rate of *n*-heptane and *iso*-octane through the whole ignition process. It is readily observed from Fig. 1b that for both RCCI and SCCI cases, overall, *n*-heptane is consumed more rapidly than *iso*-octane throughout the whole combustion process. Similar to the previous results in [31,32], the first-stage ignition delays of RCCI/SCCI combustion in the present study are nearly unchanged with the equivalence ratio and/or reactivity stratification. During the early stage of ignition, however, *n*-heptane in RCCI case is consumed slightly faster than in SCCI case, which leads to more intense first-stage ignition in RCCI case manifested in higher mean HRR during the first-stage ignition, ultimately resulting in earlier second-stage ignition.

Based on Bilger's mixture fraction [33], Z, the conditional means of HRR on Z at different times are evaluated. The results revealed that during the first-stage ignition and the start of the main combustion of RCCI case, a significant amount of heat is released from mixtures with large Z, which corresponds to local mixtures with high reactivity (high *n*-heptane concentration) and ϕ. Local mixtures with high *n*-heptane concentration ($\sim$ PRF30 with $\phi = 0.74$) auto-ignite first and then initiate the ignition of adjacent less-reactive mixtures, resulting in a sequential ignition process.

For SCCI case, the start of the main combustion is also originated from mixtures with large Z. However, these local mixtures have a lower *n*-heptane concentration (i.g., $\sim$ PRF50 with $\phi = 0.74$), and as such, less heat is released during the first-stage ignition, resulting in a delayed second-stage ignition.

It is of importance to understand the difference between chemical processes occurring in these local mixtures in RCCI and SCCI combustion. Therefore, in the next section, CEMA is applied to 0-D ignitions under the similar conditions of these local mixtures.

3.2. CEMA: 0-D ignition

As mentioned above, CEMA is applied to the 0-D ignitions of PRF30/air mixture at $p_0 = 40$ atm, $T_0 = 812$ K, and $\phi_0 = 0.74$, which corresponds to mixture with high *n*-heptane concentration with low temperature in RCCI case. Figure 2 shows the temporal evolution of temperature, λ_{exp}, EI and PI values of important species and reactions.

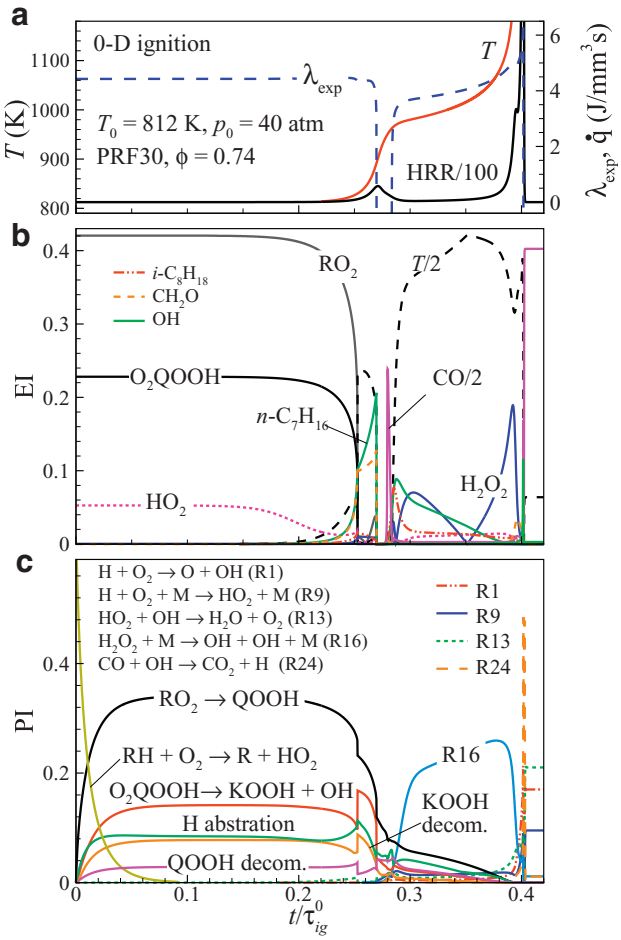

Fig. 2. Temporal evolution of (a) temperature, $\lambda_{exp} = \text{sign}(\text{Re}(\lambda_e)) \times \log(1+|\text{Re}(\lambda_e|))$, and HRR, (b) EI of important variables, and (c) PI of key elementary reactions for 0-D ignition of PRF30/air mixture.

To facilitate discussion, the schematic of overall reaction pathways of PRF oxidation under HCCI condition is shown in Fig. 3. Note that to separately evaluate the contribution of *n*-heptane and *iso*-octane to the CEM, R, Q, K, and Q′ denote radicals originated from *n*-heptane only. Several points are to be noted from the Fig. 2.

First, it is readily observed that prior to the first-stage ignition featured by positive λ_{exp}, *n*-heptane and radicals originated from *n*-heptane are the main variables contributing to CEM. As shown in Fig. 3, *n*-heptane consumption proceeds in the low-temperature chemistry (LTC) pathway: i.e., the H-atom abstraction from a fuel molecule, RH, initiates the oxidation of *n*-heptane via RH + O_2 → R + HO_2; alkyl radical, R, from RH converts into alkylperoxy radical, RO_2, via R + O_2 + M → RO_2 + M and then, the radical isomerization of RO_2 takes place to generate hydroperoxyalkyl, QOOH, via RO_2 ⇆ QOOH. QOOH converts into O_2QOOH by another O_2 addition via QOOH + O_2 → O_2QOOH. It is important to note that the chain branching reactions involving the production and decomposition of keto-hydroperoxide, KOOH, (i.e., O_2QOOH → KOOH + OH and KOOH → OH + KO) determine the overall rate of the LTC [9,34,35].

As expected from the LTC in Fig. 3, the EI and PI values in Fig. 2 also indicate that RO_2 and O_2QOOH are the most important species, and the H-atom abstraction reaction (RH + (O,OH,HO_2) → R + (OH,H_2O,H_2O_2)), isomerization of RO_2, and chain-branching decomposition of O_2QOOH are the most important reactions to CEM for the 0-D ignition of PRF30/air mixture. For 0-D ignition of PRF50/air mixture under the same initial conditions (not shown here), the above two species and three reactions are also identified as the most important species/reactions but their contribution to CEM is slightly reduced due to low *n*-heptane concentration. Due to local high concentration of

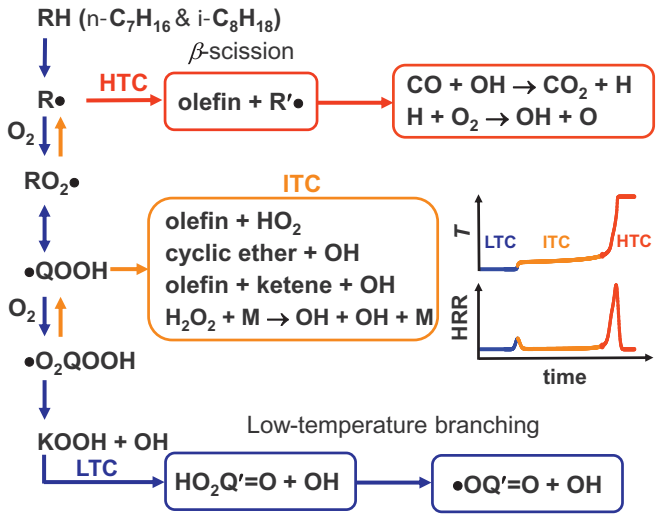

Fig. 3. Schematic of reaction pathways of *n*-heptane and *iso*-octane oxidation at different temperatures [9,34,35].

n-heptane in RCCI case, the first-stage ignition in RCCI case occurs more rapidly and more intensely than that in SCCI case under the same initial conditions as shown in Fig. 1a.

Second, near the first-stage ignition ($\sim t/\tau_{ig}^{0} = 0.27$), temperature, *n*-heptane, and CH_2O are identified as the most important variables to CEM, which is featured by the peak PIs of the chain-branching low-temperature reactions, $O_2QOOH \rightarrow KOOH + OH$ and $KOOH \rightarrow OH + KO$ (see Fig. 2c).

Third, between the first- and second-stage ignition, or in the intermediate-temperature chemistry (ITC) regime, temperature is found to be the main source of the CEM compared to *n*-heptane, *iso*-octane, and H_2O_2. During the period, the low-temperature reactions are suppressed gradually by the competing intermediate-temperature reactions of QOOH decomposition (see Fig. 3) and $H_2O_2 + M \rightarrow OH + OH + M$ (R16) is identified as the most important reaction from the PI analysis as shown in Fig. 2c. Due to the low overall reactivity of the ITC [34,35], the increase of temperature during this period becomes marginal until the second-stage ignition starts.

As temperature increases over 1000 K, the chain-branching reaction of hydrogen peroxide, $H_2O_2 + M \rightarrow OH + OH + M$ (R16), occurs very intensively, which increases temperature large enough to initiate the high-temperature chain branching reactions represented by $H + O_2 \rightarrow O + OH$. As such, temperature, CO and OH are identified as the key variables to CEM at the second-stage ignition. Meanwhile, the chain-branching reaction, $H + O_2 \rightarrow O + OH$ (R1), the conversion reaction of CO to CO_2, $CO + OH \rightarrow CO_2 + H$ (R24), and HO_2 formation reaction, $H + O_2 + M \rightarrow HO_2 + M$ (R9), are found to be the most important reactions to CEM.

It is also identified from CEMA that the ignition of PRF50/air mixture also exhibits the same characteristics as that of PRF30/air mixture except that the overall ignition is delayed due to the lower concentration of *n*-heptane in PRF50.

3.3. CEMA: 2-D DNS of RCCI/SCCI combustion

In this section, the same EI and PI analyses are applied to the 2-D DNS of RCCI/SCCI combustion to identify controlling species and reactions at two different times of the first-ignition delay, $\tau_{ig,1}$, and the onset of the main combustion at which the deflagration mode of combustion becomes dominant. The dominance of the deflagration mode of combustion was verified not only by examining the local flame structure but also by performing the Damköhler number analysis (not shown here) [16].

Figure 4 shows the isocontours of selected variables for RCCI case at $\tau_{ig,1}$, from which the key variables and reactions to the CEM can be identified at different locations. For instance, *n*-heptane and CH_2O have large EI values in relatively-low temperature regions while H_2O_2 and HO_2 have large EI values at relatively-high temperature regions. In the same way, LTC and ITC can be identified at different locations based on the PI values of important reactions. Although specific chemical information of local mixtures can be obtained from the isocontours of EI and PI values, the effects of each variable and reaction on the overall ignition and their relations are not readily observed. As such, the conditional mean of HRR, λ_{exp}, and EI/PI values of important variables/reactions for

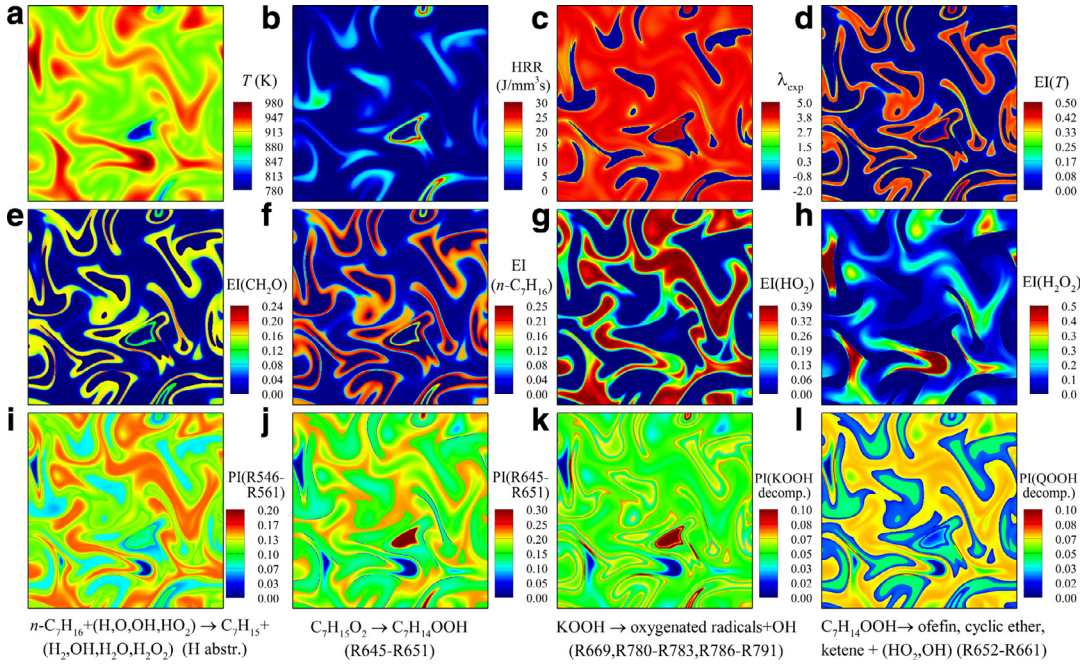

Fig. 4. Isocontours of (a) temperature, (b) HRR, (c) λ_{exp}, EI of (d) temperature and (e)–(h) critical species, and (i)–(l) PI of critical reactions at the first-ignition delay, $\tau_{ig,1}/\tau^0_{ig} = 0.22$.

both RCCI and SCCI cases at their $\tau_{ig,1}$ are shown in Fig. 5. In this study, a conditional mean value is obtained by averaging a variable conditioned on temperature to clarify the contribution of LTC, ITC, and HTC to the overall combustion. Several points are to be noted from the figure.

First, at the region where most heat is released (830 K < T < 900 K), LTC represented by the isomerization of RO_2, chain branching reactions of KOOH, and H-atom abstraction from *n*-heptane is predominant for both RCCI and SCCI combustion. As such, temperature, *n*-heptane, and CH_2O are the most important variables to the CEM. Note that at the early stage of combustion, local mixtures with low temperature correspond to high *n*-heptane concentration or low PRF number with high ϕ due to the negatively-correlated T–*n*-heptane relation. As such, these results imply that LTHR from local mixtures with relatively large ϕ is primarily responsible for temperature increase at this stage, similar to the 0-D ignition in Fig. 3. Furthermore, HRR occurs slight more intensively in RCCI case than in SCCI case, which ultimately leads to the early second-stage ignition in RCCI case.

Second, at the region with T > 900 K, the contribution of LTC to the CEM is negligible and that of ITC represented by H_2O_2 decomposition (R16) and H-atom abstraction/decomposition of *iso*-octane is significant such that no HRR occurs at this region. Consistent to the CEMA of 0-D ignition, HO_2 from QOOH decomposition and H_2O_2 via R16 are the key species for the CEM in this intermediate-temperature region.

Third, based on PI values of reactions associated with *iso*-octane decomposition in Fig. 5b, it can be conjectured that during the first-stage ignition, *iso*-octane is primarily consumed by *iso*-octane decomposition reactions at intermediate temperature region rather than by the LTC unlike the case of *n*-heptane.

In the same way, the conditional means of important variables and reactions at the time of 10% cumulative heat release rate (CHRR) for both RCCI and SCCI cases are shown in Fig. 6. On the contrary to the early stage of combustion, most heat is released from high-temperature region (T > 1500 K) where HTC represented by CO oxidation (R24) and hydrogen chemistry (R1, R9, and R13) is predominant for for both RCCI and SCCI combustion. As such, temperature, CO, and OH are identified as the most important variables to the CEM and HTHR determines temperature increase at this stage. At the region with T < 1500 K, however, the contribution of HTC to the CEM is negligible and that of ITC represented by H_2O_2 decomposition (R16) is again significant as in Figs. 5b and d such that HRR from ITC is marginal at this region.

These combustion characteristics can be further identified by the isocontours of important variables and reactions for RCCI case as in Fig. 7. It is readily observed from the figure that most HRR occurs at very thin deflagration waves where

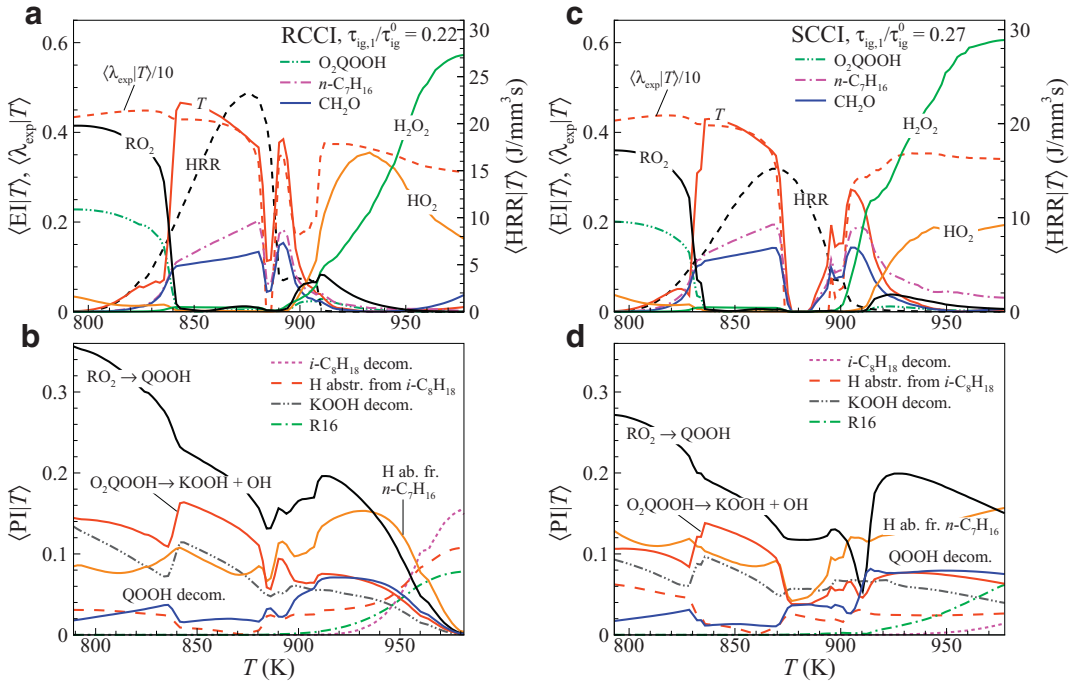

Fig. 5. Conditional mean of HRR, λ_{exp}, and EI of critical species, and PI of critical reactions at the first-stage ignition for RCCI (left column) and SCCI (right column).

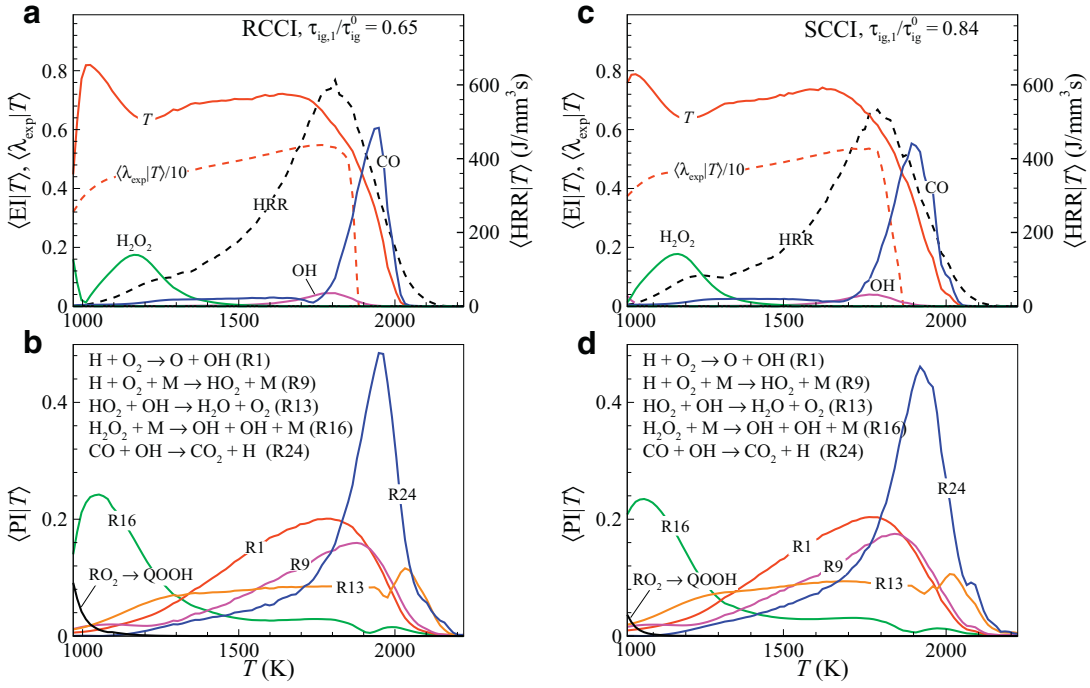

Fig. 6. Conditional means of HRR, λ_{exp} and EI of critical species, and PI of critical reactions at 10% CHRR for RCCI (left column) and SCCI (right column).

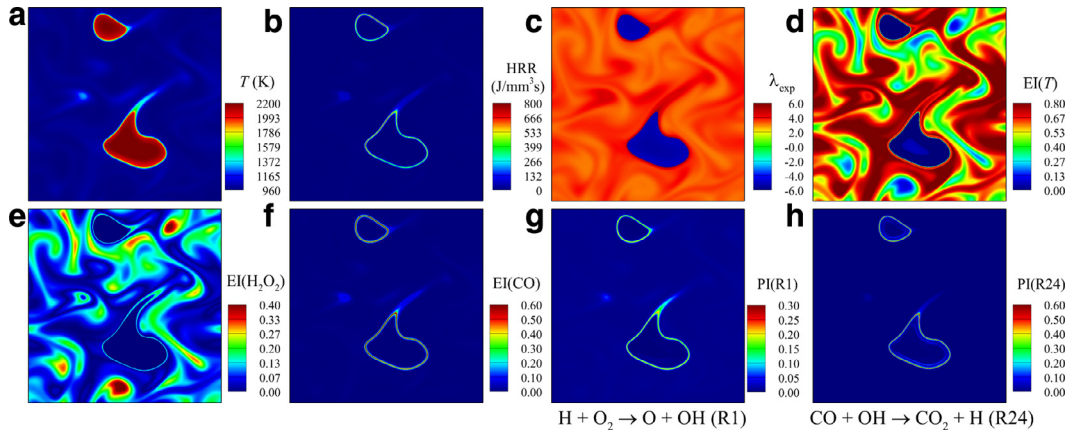

Fig. 7. Isocontours of (a) temperature, (b) HRR, (c) λ_{exp}, EI of (d) temperature and (e)–(f) critical species, and (g)–(h) PI of critical reactions at 10% CHRR, $t/\tau_{ig}^{0} = 0.65$.

the conversion reaction of CO to CO_2 and high-temperature chain-branching reaction (R1) are identified to be important to the CEM.

From a series of our DNS studies [9,16,30] together with the present study, it can be concluded that the overall RCCI/SCCI combustion can be simply understood by mapping the variation of 2-D RCCI/SCCI combustion in temperature space (Figs. 5 and 6) onto the temporal evolution of 0-D ignition (Fig. 3). However, the small difference induced by the inhomogeneities in temperature, equivalence ratio, and reactivity in 2-D DNS can significantly change its overall combustion characteristics including the overall ignition delay and mean HRR behavior, which can be used to control RCCI/SCCI combustion. For instance, the equivalence ratio and/or reactivity stratification needs to be utilized for controlling RCCI/SCCI combustion rather than temperature stratification within the negative temperature coefficient (NTC) regime. This is because the 0-D ignition delays in the NTC regime are more sensitive to the equivalence ratio and reactivity stratifications such that they can induce more deflagration waves during the early-stage of combustion, which ultimately spreads out the mean HRR more in time and reduces an excessive PRR [9,16].

4. Conclusions

The chemical characteristics of the ignition of a lean PRF/air mixture under RCCI and SCCI conditions are investigated by analyzing 2-D DNS data set with CEMA. It is found that at the first ignition delay, LTC represented by the isomerization of RO_2, chain branching reactions of KOOH, and H-atom abstraction of *n*-heptane is predominant for both RCCI and SCCI combustion. Moreover, PI and EI analyses together with conditional means of their values clarify that LTHR from mixtures with relatively-high *n*-heptane concentration occurs more intensively in RCCI combustion than in SCCI combustion, and as such, the overall RCCI combustion is more advanced in time and its mean HRR is more distributed over time than those of SCCI combustion. It is also found that at the onset of the main combustion (10% CHRR point), HTHR occurs primarily in thin deflagrations where temperature, CO, and OH are found to be the most important species for the CEM. In addition, the conversion reaction of CO to CO_2 and hydrogen chemistry including R1, R9, and R13 are identified as the most important reactions for the CEM at this stage of combustion. These overall RCCI/SCCI combustion characteristics can be simply understood by mapping the variation of 2-D RCCI/SCCI combustion in temperature space onto the temporal evolution of 0-D ignition.

Acknowledgments

This research was supported by Basic Science Research Program through the National Research Foundation of Korea (NRF) funded by the Ministry of Science, ICT & Future Planning (NRF-2015R1A2A2A01007378). SHC was supported by Saudi Aramco FUELCOM program through KAUST. This research used the resources of the KAUST Supercomputing Laboratory and UNIST Supercomputing Center.

References

[1] R.D. Reitz, G. Duraisamy, *Prog. Energy Combust. Sci.* 46 (2015) 12–71.
[2] A. Paykani, A.-H. Kakaee, P. Rahnama, R.D. Reitz, *Int. J. Engine* 17 (2016) 481–524.

[3] S.L. Kokjohn, D.A. Splitter, R.M. Hanson, R.D. Reitz, V. Manente, B. Johansson, *Atom. Sprays* 21 (2011) 107–119.
[4] S. Kokjohn, R. Reitz, D. Splitter, M. Musculus, *SAE paper* (2012) 2012–01–0375.
[5] S.L. Kokjohn, M.P.B. Musculus, R.D. Reitz, *Combust. Flame* 162 (2015) 2729–2742.
[6] C.S. Yoo, T. Lu, J.H. Chen, C.K. Law, *Combust. Flame* 158 (2011) 1727–1741.
[7] M.B. Luong, Z. Luo, T. Lu, S.H. Chung, C.S. Yoo, *Combust. Flame* 160 (2013) 2038–2047.
[8] M.B. Luong, T. Lu, S.H. Chung, C.S. Yoo, *Combust. Flame* 161 (2014) 2878–2889.
[9] M.B. Luong, G.H. Yu, T. Lu, S.H. Chung, C.S. Yoo, *Combust. Flame* 162 (2015) 4566–4585.
[10] A. Bhagatwala, R. Sankaran, S. Kokjohn, J.H. Chen, *Combust. Flame* 162 (2015) 3412–3426.
[11] C. Westbrook, *Proc. Combust. Inst.* 28 (2000) 1563–1577.
[12] W. Hwang, J.E. Dec, M. Sjöberg, *Combust. Flame* 154 (2008) 387–409.
[13] D. Splitter, S. Kokjohn, K. Rein, R. Hanson, S. Sanders, R. Reitz, *SAE paper* (2010) 2010–01–0345.
[14] S.L. Kokjohn, R.M. Hanson, D.A. Splitter, R.D. Reitz, *SAE paper* (2009) 2009–01–2647.
[15] D. Vuilleumier, D. Kozarac, M. Mehl, et al., *Combust. Flame* 161 (2014) 680–695.
[16] M.B. Luong, G.H. Yu, S.H. Chung, C.S. Yoo, *Proc. Combust. Inst.* (2016), doi:10.1016/j.proci.2016.08.038.
[17] J.H. Chen, A. Choudhary, B. de Supinski, et al., *Comput. Sci. Discov.* 2 (2009) 015001.
[18] J. Zádor, C.A. Taatjes, R.X. Fernandes, *Prog. Energy Combust. Sci.* 37 (4) (2011) 371–421.
[19] J. Zádor, H. Huang, O. Welz, J. Zetterberg, D.L. Osborn, C.A. Taatjes, *Phys. Chem. Chem. Phys.* 15 (2013) 10753–10760.
[20] C.F. Goldsmith, W.H. Green, S.J. Klippenstein, *J. Phys. Chem. A.* 116 (2012) 3325–3346.
[21] A. Miyoshi, *J. Phys. Chem. A.* 115 (2011) 3301–3325.
[22] T. Passot, A. Pouquet, *J. Fluid Mech.* 118 (1987) 441–466.
[23] T. Lu, C.S. Yoo, J.H. Chen, C.K. Law, *J. Fluid Mech.* 652 (2010) 45–64.
[24] C.S. Yoo, E.S. Richardson, R. Sankaran, J.H. Chen, *Proc. Combust. Inst.* 33 (2011) 1619–1627.
[25] Z. Luo, C.S. Yoo, E.S. Richardson, J.H. Chen, C.K. Law, T. Lu, *Combust. Flame* 159 (2012) 265–274.
[26] H. Kolla, R.W. Grout, A. Gruber, J.H. Chen, *Combust. Flame* 159 (2012) 2755–2766.
[27] A. Kazakov, M. Chaos, Z. Zhao, F.L. Dryer, *J. Phys. Chem. A.* 110 (21) (2006) 7003–7009.
[28] C.K. Law, P. Zhao, *Combust. Flame* 159 (3) (2012) 1044–1054.
[29] R. Shan, C.S. Yoo, J.H. Chen, T. Lu, *Combust. Flame* 159 (2012) 3119–3127.
[30] S.O. Kim, M.B. Luong, J.H. Chen, C.S. Yoo, *Combust. Flame* 162 (2015) 717–726.
[31] G. Mittal, M. Chaos, C.-J. Sung, F.L. Dryer, *Fuel Process. Technol.* 89 (12) (2008) 1244–1254.
[32] P. Zhao, C.K. Law, *Combust. Flame* 160 (11) (2013) 2352–2358.
[33] N. Peters, Turbulent Combustion, Cambridge University Press, 2000.
[34] H.J. Curran, P. Gaffuri, W.J. Pitz, C.K. Westbrook, *Combust. Flame* 114 (1998) 149–177.
[35] H.J. Curran, P. Gaffuri, W.J. Pitz, C.K. Westbrook, *Combust. Flame* 129 (2002) 253–280.